

1 **Ocean Surface Flux Algorithm Effects on Tropical**  
2 **Indo-Pacific Intraseasonal Precipitation**

3 **Chia-Wei Hsu<sup>1</sup>, Charlotte A. DeMott, Mark D. Branson<sup>1</sup>, Jack Reeves Eyre<sup>2</sup>,**  
4 **and Xubin Zeng<sup>3</sup>**

5 <sup>1</sup>Colorado State University, Fort Collins, CO, USA

6 <sup>2</sup>Cooperative Institute for Climate, Ocean and Ecosystem Studies, University of Washington, Seattle,  
7 WA, USA

8 <sup>3</sup>University of Arizona, Tucson, AZ, USA

9 **Key Points:**

- 10 • Latent heat flux shows significant differences between bulk flux schemes as a func-  
11 tion of wind speed and humidity disequilibrium.  
12 • Changing bulk flux schemes in model shows a more realistic latent heat flux con-  
13 tribution on maintaining precipitation.  
14 • Latent heat flux difference due to bulk flux schemes are non-uniform during dif-  
15 ferent MJO phases.

---

Corresponding author: Chia-Wei Hsu, [Chia-Wei.Hsu@colostate.edu](mailto:Chia-Wei.Hsu@colostate.edu)

**Abstract**

Surface latent heat fluxes help maintain tropical intraseasonal precipitation. We develop a latent heat flux diagnostic that depicts how latent heat fluxes vary with the near-surface specific humidity vertical gradient ( $\Delta q$ ) and surface wind speed ( $|\mathbf{V}|$ ). Compared to fluxes estimated from  $|\mathbf{V}|$  and  $\Delta q$  measured at tropical moorings and the COARE3.0 algorithm, tropical latent heat fluxes in the NCAR CEMS2 and DOE E3SMv1 models are significantly overestimated at  $|\mathbf{V}|$  and  $\Delta q$  extrema. Madden–Julian oscillation (MJO) sensitivity to surface flux algorithm is tested with offline and inline flux corrections. The offline correction adjusts model output fluxes toward mooring-estimated fluxes; the inline correction replaces the original bulk flux algorithm with the COARE3.0 algorithm in atmosphere-only simulations of each model. Both corrections reduce the latent heat flux feedback to intraseasonal precipitation, in better agreement with observations, suggesting that model-simulated fluxes are overly supportive for maintaining MJO convection.

**Plain Language Summary**

Surface latent heat flux from ocean to the atmosphere is one of the important processes that provides water vapor and energy to the daily tropical rainfall. In this study, a visually intuitive latent heat flux diagnostic is proposed to better understand the model shortfall on its latent heat flux representation. This diagnostic allows a simple assessment of model latent heat flux biases arising either from biases in water vapor or surface wind speed as well as other empirical coefficients in the model. We demonstrate that, compared to "observed" fluxes also estimated from water vapor and surface wind speed measured at tropical moorings, tropical latent heat fluxes in the NCAR CEMS2 and DOE E3SMv1 models are significantly overestimated when extreme water vapor or surface wind speed happens.

Both offline and inline latent heat flux correction is applied to simulated fluxes. For both models, the correction reduces the percentage of latent heat flux on supporting the rainfall over the tropics which is in better agreement with observations. Particularly, the latent heat flux correction are non-uniform across different stages of the Madden–Julian oscillation (MJO). This finding suggests that a model improvement on the latent heat flux representation will change the simulated MJO.

**1 Introduction**

Marine surface fluxes are the mechanism through which heat, momentum, water mass, and gases are transferred between the ocean and atmosphere. Surface sensible and latent heat fluxes play an important role in the tropical climate system by cooling the ocean surface, regulating the thermal properties of the marine boundary layer, and invigorating tropical convection through the release of latent heat when water vapor is recondensed in convective updrafts.

While equatorial latent heat fluxes are generally uncorrelated with precipitation over a wide range of scales, for some tropical disturbances, such as the Madden-Julian oscillation (MJO; Madden and Julian (1971, 1972)) and certain types of convectively-coupled equatorial waves (Kiladis et al., 2009), latent heat fluxes vary coherently with precipitation, and thus help maintain convection by replenishing column water vapor lost through precipitation formation (Dellaripa & Maloney, 2015; Yasunaga et al., 2019). Recent studies report that anomalous surface latent heat fluxes offset approximately 7–10% of column moisture lost to MJO precipitation formation (Araligidad & Maloney, 2008; Dellaripa & Maloney, 2015; DeMott et al., 2015, 2016; Bui et al., 2020). Small variations in the tropical surface latent heat flux-precipitation relationship may play an important role in regulating MJO periodicity and phase speed (Matsugishi et al., 2020), which may

then rectify onto the MJO teleconnection response that modulates the frequency of extreme weather events globally (Stan et al., 2017; Yadav & Straus, 2017).

In models, surface latent heat fluxes are parameterized using a variety of bulk flux algorithms that estimate the flux based on wind speed ( $|\mathbf{V}|$ ), the vertical gradient of near-surface specific humidity ( $\Delta q$ ), and an empirically-determined transfer coefficient. Brunke et al. (2003) demonstrated that many of the bulk flux algorithms used in modern climate models overestimate fluxes when compared to direct flux measurements from field campaigns, but the then-most recent version of the COARE algorithm (COARE3.0, hereafter referred to as COARE; (Fairall et al., 2003)) was one of the least problematic. Differences between COARE-estimated fluxes and those estimated from other widely used algorithms tend to be largest at low and high wind extremes (Zeng et al., 1998; Brodeau et al., 2017). Because winds throughout the MJO lifecycle vary from nearly calm to highly disturbed conditions (de Szoek et al., 2015), fluxes estimated using different bulk flux formulae could alter the apparent surface flux feedback to the simulated MJO.

In this study, we introduce a surface flux diagnostic that illustrates how surface latent heat fluxes vary as a function of  $|\mathbf{V}|$  and  $\Delta q$ , i.e. a “flux matrix”. The diagnostic is applied to surface fluxes estimated with in situ data from tropical Pacific moorings and the COARE algorithm. It is then applied to output from two Earth system models. We use the observational result to estimate an “offline” surface flux correction and estimate the effect of the revised flux on MJO column moistening. This offline correction is then compared to MJO-flux feedbacks in model simulations where the native bulk flux algorithm is replaced with the COARE algorithm. Models and data are described in Section 2, and results of the flux matrix analysis are presented in Section 3. Offline and inline corrections to model surface fluxes are discussed in Sections 4 and 5, respectively, and conclusions are given in Section 6.

## 2 Models and observation

We analyze daily mean surface fluxes in two Earth system models, the NCAR Community Earth System Model, version 2 (CESM2; (Danabasoglu et al., 2020)) and the DOE Energy Exascale Earth System Model, version 1 (E3SMv1; (Golaz et al., 2019)). For offline surface flux assessments, we use CESM2 output (1998-2014) from the historical (ocean-atmosphere coupled) simulation produced for phase 6 of the Coupled Model Intercomparison Project (CMIP6; (Eyring et al., 2016)) (CESM2 hereafter) and E3SMv1 output from a historical (ocean-atmosphere coupled) simulation (1995-2014) with daily output (E3SMv1 hereafter). For the inline surface flux assessment, we use the E3SMv1 atmosphere-only simulation produced by Reeves Eyre et al. (2021) where the native bulk flux algorithm is replaced with the COARE bulk flux algorithm. In their experiment, the atmosphere only simulation is forced with repeating ocean and sea-ice data based on observation year of 2000 (E3SMv1\_climo hereafter). For CESM2, we used the same code base developed by Reeves Eyre et al. (2021) for our inline experiments with a 1979-2009 AMIP-type (atmosphere-only) simulation (CESM2\_amip hereafter).

Variables needed for our analysis include the daily mean latent heat flux ( $LH$ ), rainfall ( $R$ ), 10 meter wind speed ( $|\mathbf{V}|$ ), 2 meter specific humidity ( $q_{2m}$ ), surface temperature ( $T_{sfc}$ ), and sea level pressure ( $P_{sfc}$ ). We use sea surface temperature reduced by 0.2 K (Zeng et al., 1998; Donlon & the GHRSSST-PP Science Team, 2005) to estimate the sea surface skin temperature if the simulation output does not provide surface temperature.  $T_{sfc}$  and  $P_{sfc}$  determine the saturated specific humidity ( $q_{sfc}^*$ ) at the air-sea interface which is further used to calculate the disequilibrium of moisture at the surface ( $\Delta q = 0.98q_{sfc}^* - q_{2m}$ ) where  $q_{sfc}^*$  is reduced by 0.02 to account for the reduction of  $q^*$  by salinity (Zeng et al., 1998). CESM2 in both CMIP6 and AMIP simulations provide all the listed variables. E3SMv1 CMIP6 simulation, on the other hand, provides  $|\mathbf{V}|$

114 and  $q$  at 1000 hPa. We follow de Szoeke et al. (2012) to estimate  $T_{sfc}$  and  $q_{2m}$  (See sup-  
115 plemental information for additional details).

116 For observations, we use daily means of the above fields collected with the TAO/TRITON  
117 (McPhaden et al., 1998) and RAMA (McPhaden et al., 2010) mooring arrays over the  
118 tropical Pacific and the Indian Ocean. These data are available from the National Oceanic  
119 and Atmospheric Administration Pacific Marine Environmental Laboratory at [https://](https://www.pmel.noaa.gov/gtmba/)  
120 [www.pmel.noaa.gov/gtmba/](https://www.pmel.noaa.gov/gtmba/). The latent heat flux measurement provided by the obser-  
121 vation is based on the COARE3.5 bulk flux algorithm, which is the same as COARE 3.0  
122 for latent heat flux (Edson et al., 2013). COARE is not a direct co-variance measure-  
123 ment of the surface flux, but provides one of the more accurate estimates of directly mea-  
124 sured surface fluxes (Brunke et al., 2003; Brodeau et al., 2017).

125 For intraseasonal variability and the MJO, our region of interest is the tropical In-  
126 dian Ocean and western tropical Pacific from November through April, when MJO events  
127 propagate farthest eastward (Zhang & Dong, 2004). For intraseasonal analysis, all time  
128 series are computed as anomalies from the mean annual cycle (i.e., the mean and first  
129 four harmonics) and then filtered using a 20-100 day band-pass Lanczos filter with 60  
130 weights.

### 131 3 Latent heat flux matrix

132 The bulk form of the latent heat flux ( $LH$ ) can be written as

$$LH = \rho L_v C_e |\mathbf{V}| \Delta q; \quad \Delta q = q_{sfc}^* - q_{2m} \quad (1)$$

133 where  $\rho$  is the near-surface air density,  $L_v$  is the latent heat of vaporization,  $C_e$  is the  
134 transfer coefficient, and  $|\mathbf{V}|$  and  $\Delta q$  are the same as described above. Different algorithms  
135 use different parameterizations of  $C_e$ , which varies primarily as a function of  $|\mathbf{V}|$ , with  
136 additional sensitivity to stability of the marine boundary layer (Fairall et al., 2003), wind  
137 gustiness (Redelsperger et al., 2000) and ocean wave state (Bourassa et al., 1999).

138 Based on Eq. 1, we designed a latent heat flux matrix diagnostic. Using daily mean  
139 values over the tropical Indian Ocean and western tropical Pacific (20°S–20°N and 30°E–  
140 180°E), we average the latent heat flux values based on  $|\mathbf{V}|$  with a 1  $m s^{-1}$  bin width,  
141 and  $\Delta q$  with a 1  $g kg^{-1}$  bin width (Figure 1a). We also calculate the frequency of oc-  
142 currence for each  $|\mathbf{V}|$ - $\Delta q$  bin. This diagnostic visually illustrates the relationship between  
143  $LH$ ,  $|\mathbf{V}|$ , and  $\Delta q$ , and allows for a more nuanced assessment of model latent heat flux  
144 biases than possible with seasonal mean difference maps.

145 The latent heat flux matrix from different datasets shows the discrepancies caused  
146 by the different transfer coefficients used in different bulk flux algorithms (Figure 1b-d).  
147 The latent heat flux biases from CESM2 and E3SMv1 are similar since they use the same  
148 bulk flux algorithm (Large & Yeager, 2004, 2009). The largest biases are found at ex-  
149 treme values of  $|\mathbf{V}|$  and  $\Delta q$ , indicating that the models overestimate the flux in these  
150 conditions. Small differences in biases between CESM2 and E3SMv1 likely arise from  
151 uncertainties introduced when estimating E3SMv1 near-surface  $T$ ,  $q$ , and  $|\mathbf{V}|$  values from  
152 those reported at 1000 hPa (see Supplement). For the most frequently observed condi-  
153 tions (within the 1% white contours in Figure 1), latent heat flux biases range from -20  
154  $Wm^{-2}$  to 20  $Wm^{-2}$  for both models, or 4-8% of the original latent heat flux values. These  
155 biases are statistically significant with 99% confidence.

### 156 4 Offline correction of latent heat flux and estimated effect on MJO

157 The offline correction to model latent heat fluxes is achieved by dividing all model  
158 fluxes within a given  $|\mathbf{V}|$ - $\Delta q$  bin by the model-to-mooring flux ratio for that bin. Since  
159 it is an offline correction, the changes in the latent heat flux cannot affect the precip-

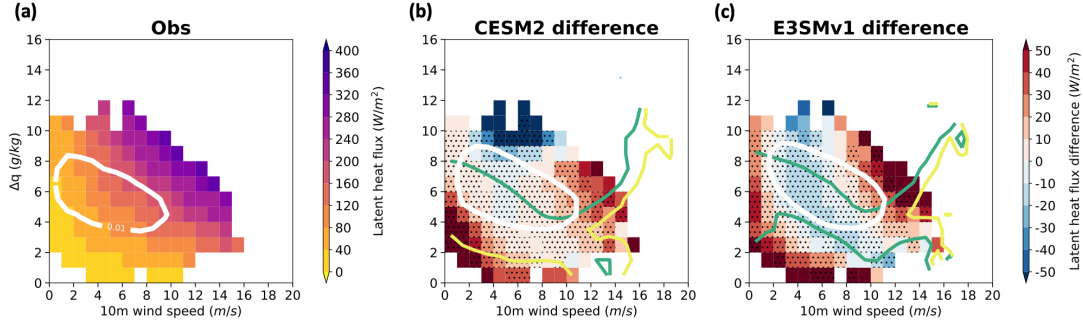


**Figure 1.** Latent heat flux (shading) binned by 10 m winds speed with 1  $m/s$  width of each bin and the moisture disequilibrium ( $\Delta q$ ) with 1  $g/kg$  width based on (a) TAO/TRITON and RAMA array over the Indian Ocean and western tropical Pacific (Obs). The same binned latent heat flux matrix subtracts the Obs’s latent heat flux matrix from (b) CESM2 and (c) E3SMv1. The dotted area means the biases are statistically significant with 99% confidence. The white thick contour line represents the probability of occurrence of 1%. The thin green and yellow contours represent the mean precipitation of 5 mm/day and 10 mm/day, respectively.

160 itation and circulations in the original simulation. This gives us a chance to quickly ex-  
 161 amine how large of a change in latent heat flux might be expected with the COARE al-  
 162 gorithm given the  $|\mathbf{V}|$  and  $\Delta q$  inputs of the existing simulation.

163 To understand how such changes to surface fluxes might affect the simulated MJO,  
 164 we regress intraseasonal latent heat flux anomalies onto intraseasonal precipitation anom-  
 165 alies, where precipitation is expressed in units of  $W\ m^{-2}$  (Figure 2). As in Bui et al. (2020),  
 166 we first focus on a small region in the western tropical Pacific ( $160^{\circ}E-180^{\circ}$  and  $10^{\circ}S-8^{\circ}S$ ).  
 167 Based on satellite-derived observational data, Bui et al. (2020) showed that intraseasonal  
 168 latent heat fluxes maintain about 7% of intraseasonal precipitation, with a correlation  
 169 of 0.79. Araligidad and Maloney (2008) and Dellaripa and Maloney (2015) found simi-  
 170 lar results with fluxes estimated with mooring data in other tropical regions.

171 Latent heat flux–precipitation regression slopes for E3SMv1 and CESM2 are shown  
 172 in Figures 2a,b. E3SMv1 and CESM2 both overestimate the regression slope for their  
 173 original flux values ( $11.3\% \pm 0.8\%$  and  $9.3\% \pm 0.6\%$ , respectively). With COARE-estimated  
 174 fluxes, E3SMv1 and CESM2 regression slopes are reduced to  $9.7\% \pm 0.7\%$  and  $8.2\% \pm$   
 175  $0.6\%$ , respectively, in closer agreement to observations. The change is statistically sig-  
 176 nificant with 99% confidence for E3SMv1, and 95% confidence for CESMs. The smaller  
 177 regression coefficient with the offline-corrected fluxes suggests that surface fluxes sim-  
 178 ulated with the original bulk flux schemes in E3SMv1 and CESM2 may artificially main-  
 179 tain intraseasonal convection in those models.

180 To explore how surface flux changes might affect intraseasonal precipitation else-  
 181 where in the Warm Pool, we calculated regression coefficients for the original and cor-  
 182 rected flux time series at each grid point for each model. The spatial patterns and mag-  
 183 nitudes of regression slope are similar between the two models (Figure 2c, d), with pos-  
 184 itive values located mainly south of the equator, consistent with the typical MJO prop-  
 185 agation pathway for this time of year (Kim et al., 2017). Changes to the regression slope  
 186 when using the offline-corrected fluxes are shown in Figure 2e, f). For E3SMv1, the of-  
 187 fline correction yields both positive and negative changes to the regression slope, while  
 188 the changes are mostly negative for CESM2.

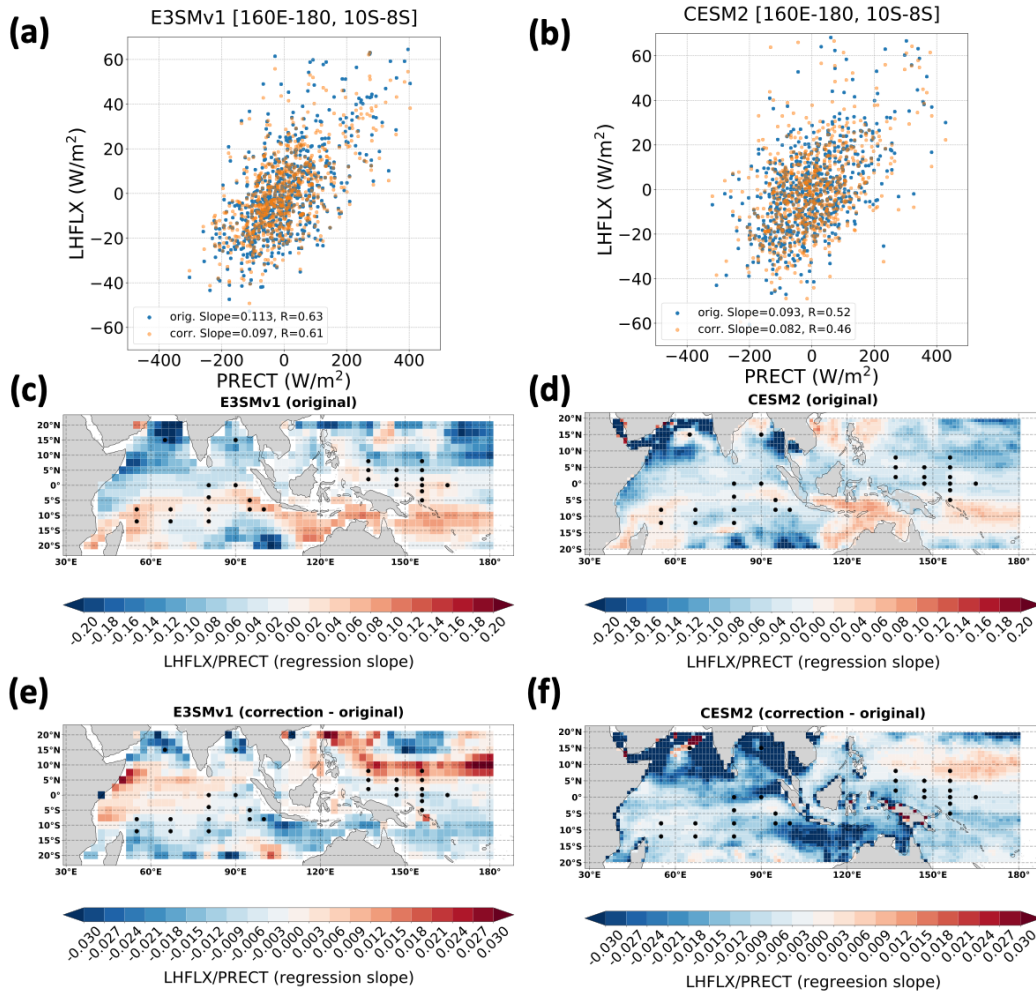


**Figure 2.** The scatter plot of November–April precipitation and latent heat flux anomalies (units of  $\text{W m}^{-2}$  for both) averaged over  $160^{\circ}\text{E}$ – $180^{\circ}$  and  $10^{\circ}\text{S}$ – $8^{\circ}\text{S}$  for (a) E3SMv1 and (b) CESM2. Blue and orange dots correspond to original and offline-corrected latent heat fluxes, respectively. The linear regression for both are shown in the legend. (c, d) maps of the regression coefficient (unitless) at each grid point for the original surface flux and (e, f) maps of regression slope changes after applying the flux correction. Black dots show locations of TAO/TRITON and RAMA moorings used to construct the flux matrix shown in Figure 1a.

189 There are at least two possible reasons for the more widespread increase of the re-  
 190 gression slope in E3SMv1 as compared to CESM2. Foremost, since the latent heat cor-  
 191 rection performed in our analysis is determined by the binned  $|\mathbf{V}|$  and  $\Delta q$ , the spatially  
 192 varying slope differences between the two models must relate to differences in the spa-  
 193 tial and temporal distributions of these variables between the two models. Some of the  
 194 difference, however, may arise from small differences in the true values of  $|\mathbf{V}|$  and  $\Delta q$   
 195 in E3SMv1 and our estimations of those quantities from their 1000 hPa surrogates (see  
 196 Supplement). However, we emphasize that the differences in regression slope changes with  
 197 flux correction are generally smaller than 3%, while the baseline regression slopes are mostly  
 198 in the range of 9–12%.

199 For both models, positive changes in regression slope are mainly located in areas  
 200 with negative regression slopes in Figure 2c and d), and vice versa. This shows that the  
 201 models tend to overestimate the magnitude of the regression slopes no matter if they are  
 202 positive or negative. Furthermore, for both models, flux correction leads to larger de-  
 203 creases in regression slopes in the subtropics (i.e., poleward of about  $10^\circ$  latitude) than  
 204 in the deep tropics ( $10^\circ\text{S}$ – $10^\circ\text{N}$ ) across the Indian Ocean and extending as far east as  
 205  $120^\circ\text{E}$ . This suggests that corrected surface fluxes for these longitudes would be less sup-  
 206 portive of intraseasonal rainfall in the subtropics than in the deep tropics.

207 Finally, we examine how flux correction might change surface fluxes within the MJO  
 208 lifecycle by regressing lagged flux and precipitation anomaly time series averaged from  
 209  $15^\circ\text{S}$ – $15^\circ\text{N}$  onto 20–100 day filtered precipitation at a base point in the eastern Indian  
 210 Ocean ( $85^\circ\text{E}$ – $95^\circ\text{E}$  and  $5^\circ\text{S}$ – $5^\circ\text{N}$ ). For the coupled simulations shown in Figure 3, MJO  
 211 precipitation in both models exhibits eastward propagation typical of many climate mod-  
 212 els (Ahn et al., 2020). Latent heat flux anomalies (shading in Figure 3) in E3SMv1 are  
 213 positive over much of the Indian Ocean from lag 0 to lag 10. In contrast, fluxes in CESM2  
 214 are mostly negative, except for smaller positive patches near the MJO convection cen-  
 215 ter at lag 0, and gradually expanding westward by lag 10. Replacing each model’s orig-  
 216 inal flux with the COARE-estimated flux yields non-uniform changes to the fluxes across  
 217 the MJO lifecycle (Figure 3c, d), reducing the flux during enhanced rainfall, and increas-  
 218 ing the flux during suppressed rainfall. In both simulations, the COARE-estimated flux  
 219 contributes less column moistening during the MJO active phase (positive rainfall anoma-  
 220 lies) and more column moistening during its suppressed phase (negative rainfall anoma-  
 221 lies). This suggests that, compared to the models’ original fluxes, COARE-estimated fluxes  
 222 would be slightly more supportive of MJO eastward propagation and less supportive of  
 223 MJO maintenance.

## 224 5 Inline correction of latent heat flux and effect on simulated MJO

225 Here, we examine the effects of the COARE algorithm on intraseasonal precipita-  
 226 tion using an inline correction. Two atmosphere-only simulations of both models were  
 227 performed, one with the original flux algorithm, and one with the COARE3.0 algorithm.  
 228 Reeves Eyre et al. (2021) provided output from the E3SM atmosphere-only simulations.  
 229 In these six-year simulations, the model was forced with a repeating cycle of observed  
 230 monthly SSTs from the year 2000. We then performed a pair of 20-year simulations with  
 231 the atmospheric component of CESM2 with the original and the COARE3.0 algorithm  
 232 using the same code modifications as in Reeves Eyre et al. (2021) and forced with ob-  
 233 served SSTs from 1979–2009. We refer to these simulations as E3SM\_climo and CESM2\_amip  
 234 to distinguish them from the coupled simulations analyzed with our offline corrections  
 235 (Section 4).

236 We find statistically significant changes with 90% confidence in the flux-precipitation  
 237 regression slope in E3SM\_climo ( $12.8\% \pm 0.7\%$  and  $11.6\% \pm 0.8\%$ , respectively) but not  
 238 in CESM2\_amip ( $12.3\% \pm 0.3\%$  and  $11.9\% \pm 0.4\%$ , respectively) in the regional aver-  
 239 aged analysis ( $160^\circ\text{E}$ – $180^\circ$  and  $10^\circ\text{S}$ – $8^\circ\text{S}$ ; Supplementary Figure 1a, b). Overestimation

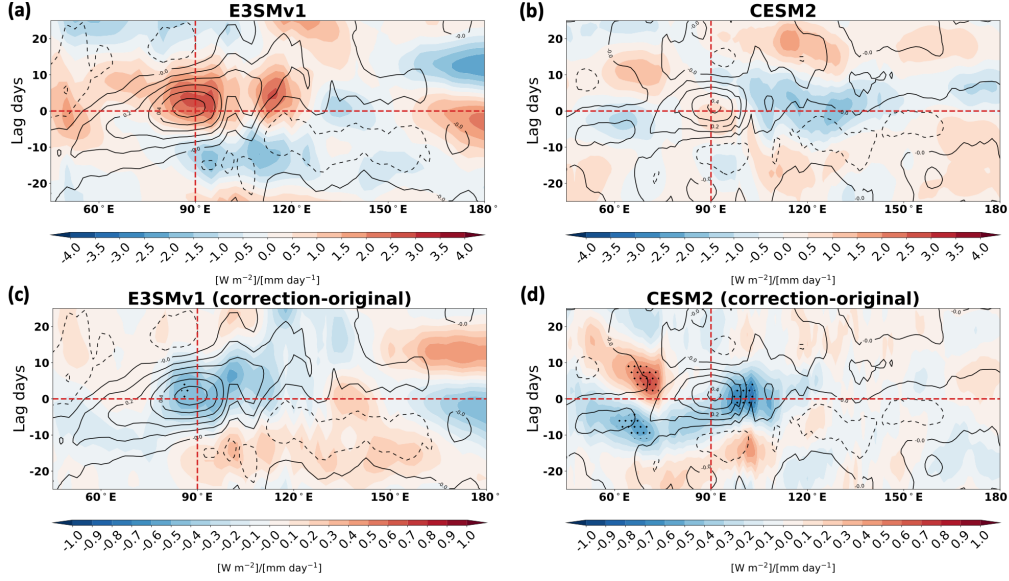


**Figure 3.** The lead-lag Hovmöller diagram of precipitation (contour with 0.1 interval) and latent heat flux (shaded) regression with base point mean precipitation ( $5^{\circ}\text{S}$ - $5^{\circ}\text{N}$  and  $85^{\circ}\text{E}$ - $95^{\circ}\text{E}$ ) during November to April in (a) E3SMv1 with original bulk flux algorithm, (b) CESM2 with original bulk flux algorithm, and offline corrected latent heat fluxes minus original latent heat fluxes in (c) E3SMv1 and (d) CESM2 with stippled regions showing the differences are significant with 90 % confidence interval.

240 of the regression slope in both models is magnified compared to the coupled simulations  
 241 (Figure 2a, b), likely due to the missing feedback of SST cooling in the coupled simu-  
 242 lations. However, both simulations show decreased regression slopes after changing to  
 243 the COARE algorithm. This effect is consistent over much of the tropics (Supplemen-  
 244 tary Figure 1c-f), but less so for E3SM\_climo, where COARE fluxes are more support-  
 245 ive of MJO convection across the equatorial Indian Ocean. With COARE, regression slopes  
 246 become slightly more positive over the Maritime Continent for both models.

247 We next examine the effect of the COARE algorithm on the evolution of intraseasonal  
 248 precipitation and surface fluxes. In contrast to the eastward propagating signal seen  
 249 in the coupled simulations (Figure 3), precipitation in the atmosphere-only simulations  
 250 exhibits distinct westward propagation for both E3SM\_climo simulations (Figure 4a, c)  
 251 and for the CESM2\_amip simulation with the original flux algorithm Figure 4b). This  
 252 is consistent with the well-known tendency for uncoupled simulations to struggle with  
 253 simulating eastward propagating intraseasonal signals compared to coupled simulations  
 254 of the same model ((DeMott et al., 2015) and references therein). For E3SM\_climo, the  
 255 effect is likely further exaggerated by a lack of interannual SST variability that has been  
 256 shown to bolster MJO eastward propagation in climate models (Klingaman & DeMott,  
 257 2020). Compared to the simulation with the original flux algorithm, the CESM2\_amip  
 258 simulation with COARE fluxes (Figure 4d) produces noticeably less westward propaga-  
 259 tion, yielding a mostly standing oscillation.

260 Changes to surface fluxes across the intraseasonal precipitation oscillation are most  
 261 apparent when comparing flux changes east and west of  $90^{\circ}\text{E}$  at lag 0. At this lag, pre-  
 262 cipitation is more suppressed to the east, and more enhanced to the west (Figures 4a-  
 263 d). Changing to the COARE flux algorithm leads to enhanced surface fluxes near and  
 264 east of precipitation and reduced fluxes west of precipitation. These changes are qual-

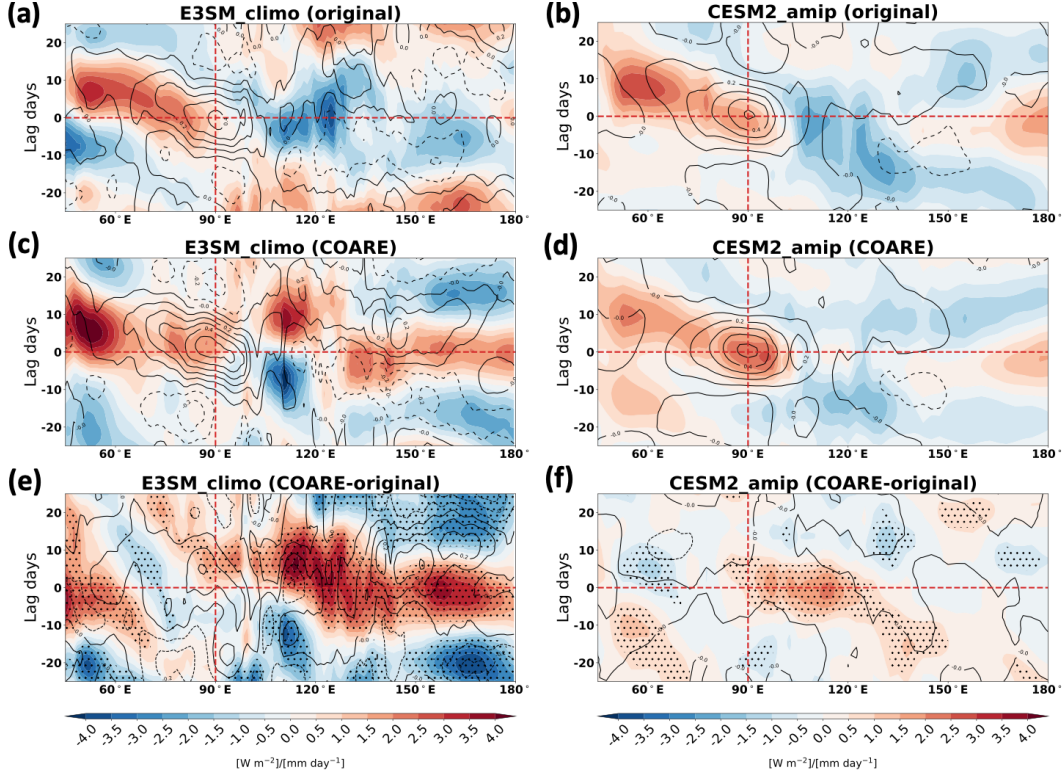


**Figure 4.** The lead-lag Hovmöller diagram of precipitation (contour with 0.1 interval) and latent heat flux (shaded) regression with base point mean precipitation ( $5^{\circ}\text{S}$ - $5^{\circ}\text{N}$  and  $85^{\circ}\text{E}$ - $95^{\circ}\text{E}$ ) during November to April in (a) E3SM\_climo with original bulk flux algorithm, (b) CESM2\_amip with original bulk flux algorithm, (c) E3SM\_climo with COARE bulk flux algorithm, (d) CESM2\_amip with COARE bulk flux algorithm, (e) (c) minuses (a), and (f) (d) minuses (b) with stippled regions showing the differences are significant with 95 % confidence interval.

265 itatively similar to those for the offline flux correction (Figure 3c, d) and offer further  
 266 support for the idea that COARE fluxes may encourage MJO eastward propagation by  
 267 enhancing column moistening to the east of precipitation and reducing it to the west.

268 **6 Summary and Conclusions**

269 In this study, we develop a simple diagnostic method to illustrate surface fluxes based  
 270 on bulk algorithm inputs ( $|\mathbf{V}|$  and  $\Delta q$ ) and then use this diagnostic to compute surface  
 271 flux biases. Compared to western tropical Pacific surface fluxes computed with in situ  
 272 observations and the COARE3.0 bulk flux algorithm, which well-estimates directly measured  
 273 surface fluxes (Brunke et al., 2003), surface fluxes in the E3SMv1 and CESM2 climate  
 274 models are too large at very low and very high wind speeds.

275 To investigate how this difference in latent heat flux might affect the MJO, we used  
 276 our flux matrix diagnostic to adjust model-simulated fluxes to COARE-estimated fluxes  
 277 within each  $|\mathbf{V}|$ - $\Delta q$  bin (i.e., the offline correction). We found that this adjustment re-  
 278 duced the latent heat flux support of intraseasonal precipitation in both models, bring-  
 279 ing it closer to observations. Longitude-lagged precipitation and latent heat flux com-  
 280 posites reveal that offline flux correction increases the flux during the MJO convectively

281 suppressed phase and reduces the flux during the MJO convectively active phase, sug-  
282 gesting that fluxes computed with the COARE algorithm are less supportive of MJO con-  
283 vection and may help promote MJO eastward propagation.

284 To test this idea, we analyzed the latent heat flux–precipitation relation in atmosphere-  
285 only simulations with E3SM\_climo and CESM2\_amip with the original and the COARE  
286 bulk flux algorithms (i.e., the inline correction). Similar to the results with the offline  
287 corrections, surface fluxes with the COARE algorithm were also less supportive of in-  
288 traseasonal convection, in better agreement with observations. The effect of COARE sur-  
289 face fluxes on the MJO propagation was difficult to assess, since both models simulate  
290 strong westward propagating disturbances in these uncoupled simulations. However, COARE  
291 fluxes in CESM2\_amip did reduce westward propagation in that model.

292 Our findings suggest that MJO simulation in climate models may be sensitive to  
293 the choice of algorithm for computing surface fluxes. This has several implications. First,  
294 as the MJO regulates extreme weather over much of the globe via teleconnections (Stan  
295 et al., 2017), changes to MJO amplitude and propagation will affect these teleconnec-  
296 tions. Second, if COARE surface fluxes contribute to enhanced MJO eastward propa-  
297 gation in fully coupled simulations, as our results here suggest they should, this could  
298 increase the number of simulated MJO events that reach the western Pacific Ocean, where  
299 its low-level westerly wind anomalies can initiate oceanic Kelvin waves that help expand  
300 the eastern edge of the Warm Pool (Puy et al., 2016) and contribute to the onset of El Niño  
301 events (Hendon et al., 2007). Finally, updating the bulk surface flux algorithm in cou-  
302 pled models will affect ocean-atmosphere coupled processes globally. Indeed, Reeves Eyre  
303 et al. (2021) found statistically significant changes to mean cloud fields and cloud radiative  
304 effects with the COARE algorithm in the E3SM\_climo experiments analyzed in our  
305 study. To explore how changes in the bulk flux algorithm are manifested in fully cou-  
306 pled simulations, we are running coupled simulations of the E3SM with the COARE bulk  
307 flux algorithm.

## 308 Acknowledgments

309 Hsu and DeMott were supported by DOE RGMA grant DE-SC0020092. DeMott  
310 also received support from NOAA MAPP NA20OAR4310389. This research used resources  
311 of the National Energy Research Scientific Computing Center (NERSC), a U.S. Depart-  
312 ment of Energy Office of Science User Facility located at Lawrence Berkeley National  
313 Laboratory, operated under Contract No. DE-AC02-05CH11231 and high-performance  
314 computing support from Cheyenne (doi:10.5065/D6RX99HX) provided by NCAR’s Com-  
315 putational and Information Systems Laboratory, sponsored by the National Science Foun-  
316 dation.

317 TAO mooring data were provided by the Global Tropical Moored Buoy Array (<https://www.pmel.noaa.gov/tao/drupal/disdel/>). E3SM Project, DOE. Energy Exascale Earth  
318 System Model v1.0. Computer Software is available at <https://github.com/E3SM-Project/E3SM/releases/tag/v1.0.0> since 23 Apr. 2018 with Web doi:10.11578/E3SM/dc.20180418.36.  
319 and the raw model output is available at <https://portal.nersc.gov/archive/home/j/jeyre/www/>. Instruction for downloading CESM2 model code can be found at <https://www.cesm.ucar.edu/models/cesm2/release/download.html> and the raw model out-  
320 put can be found at Earth System Grid Federation at <https://esgf-node.llnl.gov/projects/cmip6/>. Data used to create the figures in this article are available at <http://dx.doi.org/10.25675/10217/234033>.  
321  
322  
323  
324  
325  
326

## 327 References

328 Ahn, M.-S., Kim, D., Kang, D., Lee, J., Sperber, K. R., Gleckler, P. J., . . . Kim,  
329 H. (2020). MJO Propagation Across the Maritime Continent: Are CMIP6

- 330 Models Better Than CMIP5 Models? *Geophysical Research Letters*, 47(11),  
 331 e2020GL087250. doi: 10.1029/2020GL087250
- 332 Araligidad, N. M., & Maloney, E. D. (2008). Wind-driven latent heat flux and the  
 333 intraseasonal oscillation. *Geophysical Research Letters*, 35(4). doi: 10.1029/  
 334 2007GL032746
- 335 Bourassa, M. A., Vincent, D. G., & Wood, W. L. (1999, May). A Flux Pa-  
 336 rameterization Including the Effects of Capillary Waves and Sea State.  
 337 *Journal of the Atmospheric Sciences*, 56(9), 1123–1139. doi: 10.1175/  
 338 1520-0469(1999)056<1123:AFPITE>2.0.CO;2
- 339 Brodeau, L., Barnier, B., Gulev, S. K., & Woods, C. (2017, January). Climatologi-  
 340 cally Significant Effects of Some Approximations in the Bulk Parameterizations  
 341 of Turbulent Air–Sea Fluxes. *Journal of Physical Oceanography*, 47(1), 5–28.  
 342 doi: 10.1175/JPO-D-16-0169.1
- 343 Brunke, M. A., Fairall, C. W., Zeng, X., Eymard, L., & Curry, J. A. (2003, Febru-  
 344 ary). Which Bulk Aerodynamic Algorithms are Least Problematic in Comput-  
 345 ing Ocean Surface Turbulent Fluxes? *Journal of Climate*, 16(4), 619–635. doi:  
 346 10.1175/1520-0442(2003)016<0619:WBAAAL>2.0.CO;2
- 347 Bui, H. X., Maloney, E. D., Dellaripa, E. M. R., & Singh, B. (2020). Wind  
 348 Speed, Surface Flux, and Intraseasonal Convection Coupling From CYGNSS  
 349 Data. *Geophysical Research Letters*, 47(21), e2020GL090376. doi:  
 350 10.1029/2020GL090376
- 351 Danabasoglu, G., Lamarque, J.-F., Bacmeister, J., Bailey, D. A., DuVivier, A. K.,  
 352 Edwards, J., ... Strand, W. G. (2020). The Community Earth System Model  
 353 Version 2 (CESM2). *Journal of Advances in Modeling Earth Systems*, 12(2),  
 354 e2019MS001916. doi: 10.1029/2019MS001916
- 355 Dellaripa, E. M. R., & Maloney, E. D. (2015). Analysis of MJO Wind-Flux  
 356 Feedbacks in the Indian Ocean Using RAMA Buoy Observations. *Journal*  
 357 *of the Meteorological Society of Japan. Ser. II*, 93A, 1–20. doi: 10.2151/  
 358 jmsj.2015-021
- 359 DeMott, C. A., Benedict, J. J., Klingaman, N. P., Woolnough, S. J., & Randall,  
 360 D. A. (2016). Diagnosing ocean feedbacks to the MJO: SST-modulated surface  
 361 fluxes and the moist static energy budget. *Journal of Geophysical Research:*  
 362 *Atmospheres*, 121(14), 8350–8373. doi: 10.1002/2016JD025098
- 363 DeMott, C. A., Klingaman, N. P., & Woolnough, S. J. (2015). Atmosphere-ocean  
 364 coupled processes in the Madden-Julian oscillation. *Reviews of Geophysics*,  
 365 53(4), 1099–1154. doi: 10.1002/2014RG000478
- 366 de Szoeki, S. P., Edson, J. B., Marion, J. R., Fairall, C. W., & Bariteau, L. (2015,  
 367 January). The MJO and Air–Sea Interaction in TOGA COARE and DY-  
 368 NAMO. *Journal of Climate*, 28(2), 597–622. doi: 10.1175/JCLI-D-14-00477.1
- 369 de Szoeki, S. P., Yuter, S., Mechem, D., Fairall, C. W., Burleyson, C. D., &  
 370 Zuidema, P. (2012, December). Observations of Stratocumulus Clouds and  
 371 Their Effect on the Eastern Pacific Surface Heat Budget along 20°S. *Journal of*  
 372 *Climate*, 25(24), 8542–8567. doi: 10.1175/JCLI-D-11-00618.1
- 373 Donlon, C. J., & the GHRSSST-PP Science Team. (2005). *The Recommended*  
 374 *GHRSSST-PP Data Processing Specification GDS (version 1 revision 1.6)*. The  
 375 GHRSSST-PP International Project Office, Exeter, U.K.
- 376 Edson, J. B., Jampana, V., Weller, R. A., Bigorre, S. P., Plueddemann, A. J.,  
 377 Fairall, C. W., ... Hersbach, H. (2013, August). On the Exchange of Mo-  
 378 mentum over the Open Ocean. *Journal of Physical Oceanography*, 43(8),  
 379 1589–1610. doi: 10.1175/JPO-D-12-0173.1
- 380 Eyring, V., Bony, S., Meehl, G. A., Senior, C. A., Stevens, B., Stouffer, R. J., &  
 381 Taylor, K. E. (2016, May). Overview of the Coupled Model Intercomparison  
 382 Project Phase 6 (CMIP6) experimental design and organization. *Geoscientific*  
 383 *Model Development*, 9(5), 1937–1958. doi: 10.5194/gmd-9-1937-2016
- 384 Fairall, C. W., Bradley, E. F., Hare, J. E., Grachev, A. A., & Edson, J. B. (2003,

- February). Bulk Parameterization of Air–Sea Fluxes: Updates and Verification for the COARE Algorithm. *Journal of Climate*, *16*(4), 571–591. doi: 10.1175/1520-0442(2003)016<0571:BPOASF>2.0.CO;2
- Golaz, J.-C., Caldwell, P. M., Roedel, L. P. V., Petersen, M. R., Tang, Q., Wolfe, J. D., ... Zhu, Q. (2019). The DOE E3SM Coupled Model Version 1: Overview and Evaluation at Standard Resolution. *Journal of Advances in Modeling Earth Systems*, *11*(7), 2089–2129. doi: 10.1029/2018MS001603
- Hendon, H. H., Wheeler, M. C., & Zhang, C. (2007, February). Seasonal Dependence of the MJO–ENSO Relationship. *Journal of Climate*, *20*(3), 531–543. doi: 10.1175/JCLI4003.1
- Kiladis, G. N., Wheeler, M. C., Haertel, P. T., Straub, K. H., & Roundy, P. E. (2009). Convectively coupled equatorial waves. *Reviews of Geophysics*, *47*(2). doi: 10.1029/2008RG000266
- Kim, D., Kim, H., & Lee, M.-I. (2017). Why does the MJO detour the Maritime Continent during austral summer? *Geophysical Research Letters*, *44*(5), 2579–2587. doi: 10.1002/2017GL072643
- Klingaman, N. P., & DeMott, C. A. (2020). Mean State Biases and Interannual Variability Affect Perceived Sensitivities of the Madden-Julian Oscillation to Air–Sea Coupling. *Journal of Advances in Modeling Earth Systems*, *12*(2), e2019MS001799. doi: 10.1029/2019MS001799
- Large, W. G., & Yeager, S. G. (2004). *Diurnal to Decadal Global Forcing for Ocean and Sea-Ice Models: The Data Sets and Flux Climatologies*. NCAR Tech. Note NCAR/TN-460+STR, University Corporation for Atmospheric Research.
- Large, W. G., & Yeager, S. G. (2009, August). The global climatology of an interannually varying air–sea flux data set. *Clim Dyn*, *33*(2), 341–364. doi: 10.1007/s00382-008-0441-3
- Madden, R. A., & Julian, P. R. (1971, July). Detection of a 40–50 Day Oscillation in the Zonal Wind in the Tropical Pacific. *Journal of the Atmospheric Sciences*, *28*(5), 702–708. doi: 10.1175/1520-0469(1971)028<0702:DOADOI>2.0.CO;2
- Madden, R. A., & Julian, P. R. (1972, September). Description of Global-Scale Circulation Cells in the Tropics with a 40–50 Day Period. *Journal of the Atmospheric Sciences*, *29*(6), 1109–1123. doi: 10.1175/1520-0469(1972)029<1109:DOGSCC>2.0.CO;2
- Matsugishi, S., Miura, H., Nasuno, T., & Satoh, M. (2020). Impact of latent heat flux modifications on the reproduction of a Madden–Julian oscillation event during the 2015 Pre-YMC campaign using a global cloud-system-resolving model. *Sola, advpub*. doi: 10.2151/sola.16A-003
- McPhaden, M., Ando, K., Bourles, B., Freitag, H., Lumpkin, R., Masumoto, Y., ... Yu, W. (2010, December). The Global Tropical Moored Buoy Array. In *Proceedings of OceanObs’09: Sustained Ocean Observations and Information for Society* (pp. 668–682). European Space Agency. doi: 10.5270/OceanObs09.cwp.61
- McPhaden, M., Busalacchi, A., Cheney, R., Donguy, J., Gage, K., Halpern, D., ... Takeuchi, K. (1998). The Tropical Ocean–Global Atmosphere observing system: A decade of progress. doi: 10.1029/97JC02906
- Puy, M., Vialard, J., Lengaigne, M., & Guilyardi, E. (2016, April). Modulation of equatorial Pacific westerly/easterly wind events by the Madden–Julian oscillation and convectively-coupled Rossby waves. *Clim Dyn*, *46*(7), 2155–2178. doi: 10.1007/s00382-015-2695-x
- Redelsperger, J.-L., Guichard, F., & Mondon, S. (2000, January). A Parameterization of Mesoscale Enhancement of Surface Fluxes for Large-Scale Models. *Journal of Climate*, *13*(2), 402–421. doi: 10.1175/1520-0442(2000)013<0402:APOME0>2.0.CO;2

- 440 Reeves Eyre, J. E. J., Zeng, X., & Zhang, K. (2021). Ocean Surface Flux Algorithm  
441 Effects on Earth System Model Energy and Water Cycles. *Front. Mar. Sci.*, 8.  
442 doi: 10.3389/fmars.2021.642804
- 443 Stan, C., Straus, D. M., Frederiksen, J. S., Lin, H., Maloney, E. D., & Schu-  
444 macher, C. (2017). Review of Tropical-Extratropical Teleconnections on  
445 Intraseasonal Time Scales. *Reviews of Geophysics*, 55(4), 902–937. doi:  
446 10.1002/2016RG000538
- 447 Yadav, P., & Straus, D. M. (2017, May). Circulation Response to Fast and Slow  
448 MJO Episodes. *Monthly Weather Review*, 145(5), 1577–1596. doi: 10.1175/  
449 MWR-D-16-0352.1
- 450 Yasunaga, K., Yokoi, S., Inoue, K., & Mapes, B. E. (2019, January). Space–Time  
451 Spectral Analysis of the Moist Static Energy Budget Equation. *Journal of Cli-  
452 mate*, 32(2), 501–529. doi: 10.1175/JCLI-D-18-0334.1
- 453 Zeng, X., Zhao, M., & Dickinson, R. E. (1998, October). Intercomparison of Bulk  
454 Aerodynamic Algorithms for the Computation of Sea Surface Fluxes Using  
455 TOGA COARE and TAO Data. *Journal of Climate*, 11(10), 2628–2644. doi:  
456 10.1175/1520-0442(1998)011<2628:IOBAAF>2.0.CO;2
- 457 Zhang, C., & Dong, M. (2004, August). Seasonality in the Madden–Julian Oscilla-  
458 tion. *Journal of Climate*, 17(16), 3169–3180. doi: 10.1175/1520-0442(2004)  
459 017<3169:SITMO>2.0.CO;2